PHYSICAL REVIEW E **71**, 060102(R) (2005)

Flux reversal in a two-state symmetric optical thermal ratchet

Sang-Hyuk Lee and David G. Grier
Department of Physics and Center for Soft Matter Research, New York University, New York, New York 10003, USA
(Received 4 February 2005; revised manuscript received 4 April 2005; published 29 June 2005)

A Brownian particle's random motions can be rectified by a periodic potential-energy landscape that alternates between two states, even if both states are spatially symmetric. If the two states differ only by a discrete translation, the direction of the ratchet-driven current can be reversed by changing their relative durations. We experimentally demonstrate flux reversal in a symmetric two-state ratchet by tracking the motions of colloidal spheres moving through large arrays of discrete potential-energy wells created with dynamic holographic optical tweezers. The model's simplicity and high degree of symmetry suggest possible applications in molecular-scale motors.

DOI: 10.1103/PhysRevE.71.060102 PACS number(s): 05.60.Cd, 82.70.Dd, 87.80.Cc

Until fairly recently, random thermal fluctuations were considered impediments to inducing motion in systems such as motors. Fluctuations can be harnessed, however, through mechanisms such as stochastic resonance [1] and thermal ratchets [2], as efficient transducers of input energy into mechanical motion. Unlike conventional machines, which battle noise, molecular-scale devices that exploit these processes actually requite thermal fluctuations to operate.

This article focuses on thermal ratchets in which the random motions of Brownian particles are rectified by a time-varying potential-energy landscape. Even when the landscape has no overall slope and thus exerts no average force, directed motion still can result from the accumulation of coordinated impulses. Most thermal ratchet models break spatiotemporal symmetry by periodically translating, tilting, or otherwise modulating a spatially asymmetric landscape [2]. Inducing a flux is almost inevitable in such systems unless they satisfy conditions of spatiotemporal symmetry or supersymmetry [3]. Even a spatially symmetric landscape can induce a flux with appropriate driving [4–7]. Unlike deterministic motors, however, the direction of motion in these systems can depend sensitively on implementation details.

We recently demonstrated a spatially symmetric three-state thermal ratchet for micrometer-scale colloidal particles implemented with arrays of holographic optical tweezers, each of which constitutes a discrete potential-energy well [7]. Repeatedly displacing the array, first by one-third of a lattice constant and then by two-thirds, breaks spatiotemporal symmetry in a manner that induces a flux. Somewhat surprisingly, the *direction* of motion depends sensitively on the duration of the states relative to the time required for a particle to diffuse the intertrap separation [7]. The induced flux therefore can be canceled or even reversed by varying the rate of cycling, rather than the direction. This approach builds upon the pioneering demonstration of unidirectional flux induced by a spatially asymmetric time-averaged optical ratchet [8,9], and of reversible transitions driven by stochastic resonance in a dual-trap rocking ratchet [10,11].

Here, we demonstrate flux induction and flux reversal in a symmetric *two-state* thermal ratchet implemented with dynamic holographic optical trap arrays [12,13]. The transport mechanism for this two-state ratchet is more subtle than our previous three-state model in that the direction of motion is not easily intuited from the protocol. Its capacity for flux reversal in the absence of external loading, by contrast, can be inferred immediately by considerations of spatiotemporal symmetry. This also differs from the three-state ratchet [7] and the rocking double tweezer [10,11] in which flux reversal results from a finely tuned balance of parameters.

Figure 1 schematically depicts how the two-state ratchet operates. Each state consists of a pattern of discrete optical traps, modeled here as Gaussian wells of width σ and depth V_0, uniformly separated by a distance $L \gg \sigma$. The first array of traps is extinguished after time T_1 and replaced immediately with a second array, which is displaced from the first by $L/3$. The second pattern is extinguished after time T_2 and replaced again by the first, thereby completing one cycle.

If the potential wells in the second state overlap those in the first, then trapped particles are handed back and forth between neighboring traps as the states cycle, and no motion results. This also is qualitatively different from the three-state ratchet, which deterministically transfers particles forward under comparable conditions, in a process known as optical peristalsis [7,14]. The only way the symmetric two-state ratchet can induce motion is if trapped particles are released when the states change and then diffuse freely.

The motion of a Brownian particle in this system can be described with the one-dimensional Langevin equation

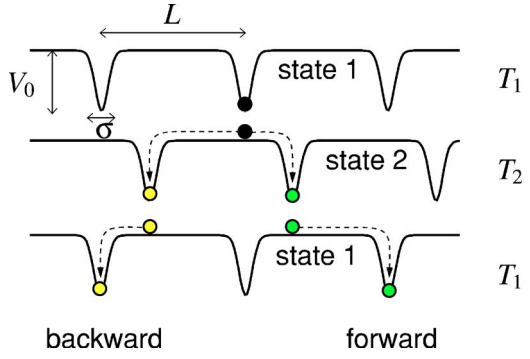

FIG. 1. One complete cycle of a spatially symmetric two-state ratchet potential comprised of discrete potential wells.

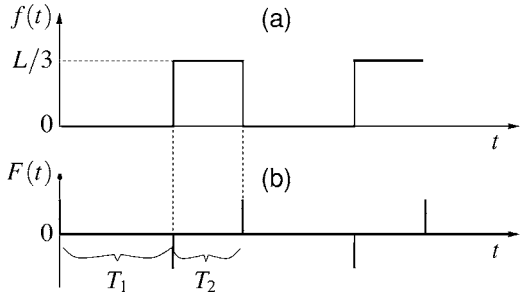

FIG. 2. (a) Displacement function $f(t)$. (b) Equivalent tilting-ratchet driving force, $F(t)=-\eta\dot{f}(t)$.

$$\eta\dot{x}(t) = -V'(x(t)-f(t)) + \xi(t), \tag{1}$$

where η is the particle's viscous drag coefficient, $V(x)$ is the potential-energy landscape, $V'(x)=\partial V(x)/\partial x$ is its derivative, and $\xi(t)$ is a δ-correlated stochastic force representing thermal noise. The potential-energy landscape in our system is spatially periodic with period L,

$$V(x+L) = V(x). \tag{2}$$

The time-varying displacement of the potential energy in our two-state ratchet is described by a periodic function $f(t)$ with period $T=T_1+T_2$, which is plotted in Fig. 2(a).

The equations describing this traveling potential ratchet can be recast into the form of a tilting ratchet, which ordinarily would be implemented by applying an oscillatory external force to objects on an otherwise fixed landscape. The appropriate coordinate transformation, $y(t)=x(t)-f(t)$ [2], yields

$$\eta\dot{y}(t) = -V'(y(t)) + F(t) + \xi(t), \tag{3}$$

where $F(t)=-\eta\dot{f}(t)$ is the effective driving force. Because $f(t)$ has a vanishing mean, the average velocity of the original problem is the same as that of the transformed tilting ratchet $\langle\dot{x}\rangle=\langle\dot{y}\rangle$, where the angle brackets imply both an ensemble average and an average over a period T.

Reimann has demonstrated [2,3] that a steady-state flux, $\langle\dot{y}\rangle\neq 0$, develops in any tilting ratchet that breaks both spatiotemporal symmetry,

$$V(y) = V(-y) \quad \text{and} \quad -F(t) = F(t+T/2), \tag{4}$$

and also spatiotemporal supersymmetry,

$$-V(y) = V(y+L/2) \quad \text{and} \quad -F(t+\Delta t) = F(-t), \tag{5}$$

for any Δt. No flux results if either of Eqs. (4) and (5) is satisfied.

The optical trapping potential depicted in Fig. 1 is symmetric but not supersymmetric. Provided that $F(t)$ violates the symmetry condition in Eq. (4), the ratchet must induce directed motion. Although $F(t)$ is supersymmetric, as can be seen in Fig. 2(b), it is symmetric only when $T_1=T_2$. Consequently, we expect a particle current for $T_1\neq T_2$. The zero crossing at $T_1=T_2$ furthermore portends flux reversal on either side of the equality.

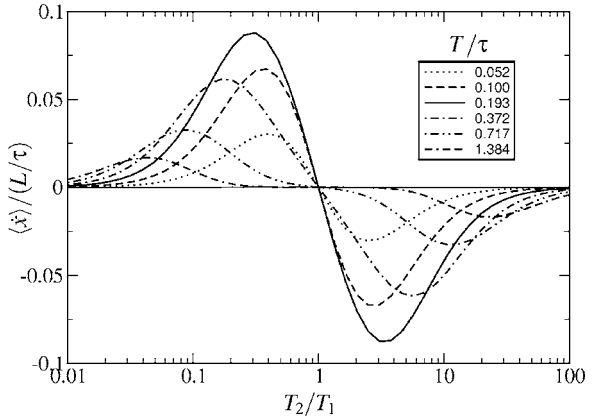

FIG. 3. Steady-state drift velocity as a function of the relative dwell time, T_2/T_1, for $\beta V_0=2.75$, $L=5.2$ μm, $\sigma=0.65$ μm, and various values of T/τ. Transport is optimized under these conditions by running the ratchet at $T/\tau=0.193$.

We calculate the steady-state velocity for this system by solving the master equation associated with Eq. (1) [7,15]. The probability for a driven Brownian particle to drift from position x_0 to within dx of position x during the interval t, is given by the propagator

$$P(x,t|x_0,0)dx = e^{\int^t L(x,t')dt'}\delta(x-x_0)dx, \tag{6}$$

where the Liouville operator is

$$L(x,t) = D\left(\frac{\partial^2}{\partial x^2} + \beta\frac{\partial}{\partial x}V'(x,t)\right), \tag{7}$$

and where β^{-1} is the thermal energy scale [15]. The steady-state particle distribution $\rho(x)$ is an eigenstate of the master equation

$$\rho(x) = \int P(x,T|x_0,0)\rho(x_0)dx_0, \tag{8}$$

and the associated steady-state flux is [7]

$$v = \int \frac{x-x_0}{T}\rho(x_0)P(x,T|x_0,0)dxdx_0. \tag{9}$$

The natural length scale in this problem is L, the intertrap spacing in either state. The natural time scale, $\tau=L^2/(2D)$, is the time required for particles of diffusion constant D to diffuse this distance.

Figure 3 shows how v varies with T_2/T_1 for various values of T/τ for experimentally accessible values of V_0, σ, and L. As anticipated, the net drift vanishes for $T_1=T_2$. Less obviously, the induced flux is directed from each well in the longer-duration state toward the nearest well in the short-lived state. The flux falls off as $1/T$ in the limit of large T because the particles spend increasingly much of their time localized in traps. It also diminishes for short T because the particles cannot keep up with the landscape's evolution. In between, the range of fluxes can be tuned with T.

We implemented this model for a sample of 1.53-μm-diam colloidal silica spheres (Bangs Laboratories, lot number 5328) dispersed in water, using potential-energy

landscapes created from arrays of holographic optical traps [7,12,13,16]. The sample was enclosed in a hermetically sealed glass chamber roughly 40-μm thick created by bonding the edges of a coverslip to a microscope slide, and was allowed to equilibrate to room temperature (21±1 °C) on the stage of a Zeiss S100 2TV Axiovert inverted optical microscope. A 100×NA 1.4 oil immersion SPlan Apo objective lens was used to focus the optical tweezer array into the sample and to image the spheres, whose motions were captured with an NEC TI 324A low noise monochrome charge-coupled device (CCD) camera. The micrograph in Fig. 4(a) shows the focused light from a 5×20 array of optical traps formed by a phase hologram projected with a Hamamatsu X7550 spatial light modulator [17]. The tweezers are arranged in twenty-trap manifolds 37-μm long separated by L=5.2 μm. Each trap is powered by an estimated 2.5±0.4 mW of laser light at 532 nm. The particles, which appear in the bright-field micrograph in Fig. 4(b), are twice as dense as water and sediment to the lower glass surface, where they diffuse freely in the plane with a measured diffusion coefficient of D=0.33±0.03 μm^2/sec. This establishes the characteristic time scale for the system of τ =39.4 sec, which is quite reasonable for digital video microscopy studies. Out-of-plane fluctuations were minimized by focusing the traps at the spheres' equilibrium height above the wall [18].

We projected two-state cycles of optical trapping patterns in which the manifolds in Fig. 4(a) were alternately displaced in the spheres' equilibrium plane by $L/3$, with the duration of the first state fixed at T_1=3 sec and T_2 ranging from 0.8 to 14.7 sec. To measure the flux induced by this cycling potential-energy landscape for one value of T_2, we first gathered roughly two dozen particles in the middle row of traps in state 1, as shown in Fig. 4(b), and then projected up to one hundred periods of two-state cycles. The particles' motions were recorded as uncompressed digital video streams for analysis [19]. Their time-resolved trajectories then were averaged over the transverse direction into the probability density, $\rho(x,t)\Delta x$, for finding particles within Δx=0.13 μm of position x after time t. We also tracked particles outside the trapping pattern to monitor their diffusion coefficients and to ensure the absence of drifts in the supporting fluid. Starting from this well-controlled initial condition resolves any uncertainties arising from the evolution of nominally random initial conditions [7].

Figures 4(c) and 4(d) show the spatially resolved time evolution of $\rho(x,t)$ for T_2=0.8 sec$<T_1$ and T_2=8.6 sec $>T_1$. In both cases, the particles spend most of their time localized in traps, visible here as bright stripes, occasionally using the shorter-lived traps as springboards to neighboring wells in the longer-lived state. The mean particle position $\langle x(t)\rangle = \int x\rho(x,t)dx$ advances as the particles make these jumps, with the associated results plotted in Fig. 4(e).

The speed with which an initially localized state, $\rho(x,0) \approx \delta(x)$, advances differs from the steady-state speed plotted, in Fig. 3, but still can be calculated as the first moment of the propagator,

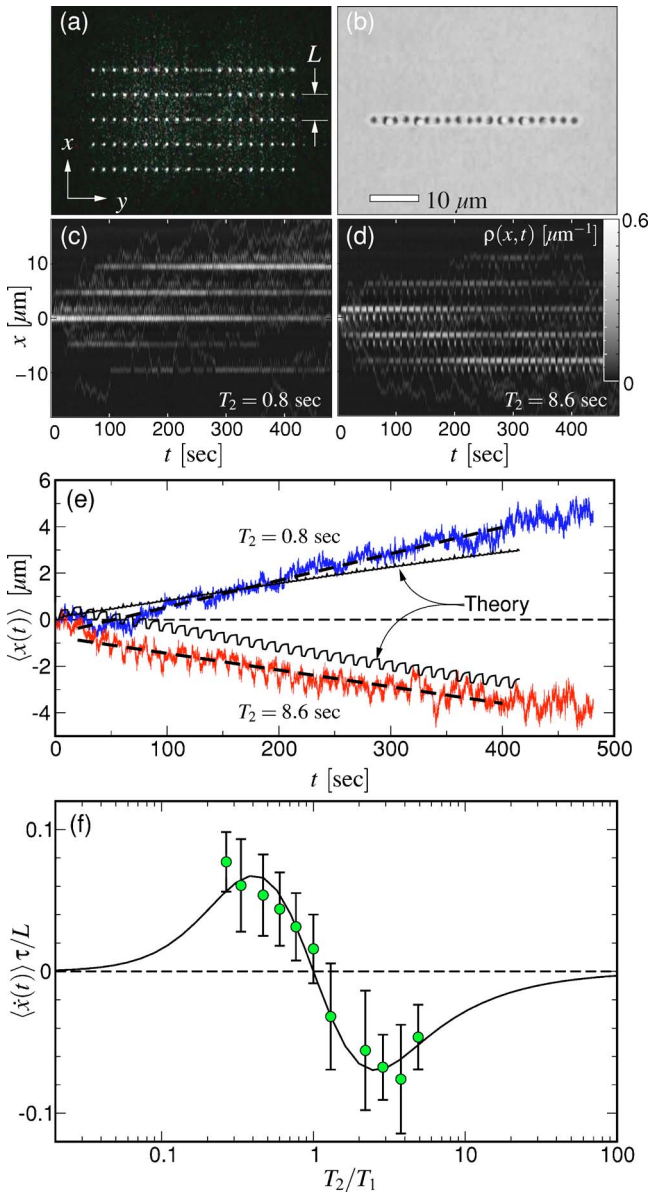

FIG. 4. (a) Image of 5×20 array of holographic optical traps at L=5.2 μm. (b) Video micrograph of colloidal silica spheres 1.53 μm in diameter trapped in the middle row of the array at the start of an experimental run. (c) and (d) Time evolution of the measured probability density for finding particles at T_2=0.8 sec and T_2=8.6 sec, respectively, with T_1 fixed at 3 sec. (e) Time evolution of the particles' mean position calculated from the distribution functions in (c) and (d). The slopes of linear fits provide estimates for the induced drift velocity, which can be compared with displacements calculated with Eq. (10) for βV_0=2.75 and σ=0.65 μm. (f) Measured drift speed as a function of relative dwell time T_2/T_1, compared with predictions of Eq. (9).

$$\langle x(t)\rangle = \int yP(y,t|0,0)dy. \tag{10}$$

Numerical analysis reveals a nearly constant mean speed that agrees quite closely with the steady-state speed from Eq. (9).

Fitting traces such as those in Fig. 4(e) to linear trends

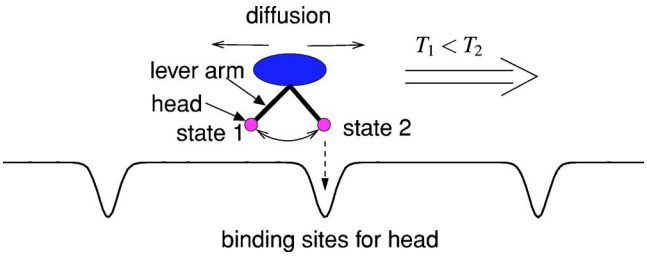

FIG. 5. Toy model of diffusive molecular motor.

provides estimates for the ratchet-induced flux, which is plotted in Fig. 4(f). The solid curve in Fig. 4(f) shows excellent agreement with predictions of Eq. (10) for $\beta V_0 = 2.75 \pm 0.5$ and $\sigma = 0.65 \pm 0.05$ μm.

Our implementation of the two-state ratchet involves updating the optical intensity pattern to translate the physical landscape. However, the same principles can be applied to systems in which the landscape remains fixed and the object undergoes cyclic transitions between two states. Figure 5 depicts a model for an active two-state walker on a fixed physical landscape that is inspired by the biologically relevant transport of single myosin head groups along actin filaments [20]. The walker consists of a head group that interacts with localized potential-energy wells periodically distributed on the landscape. It also is attached to a lever arm that uses an external energy source to translate the head group by a distance somewhat smaller than the interwell separation. The other end of the lever arm is connected to the payload, whose viscous drag would provide the leverage necessary to translate the head group between the extended and retracted states. Switching between the walker's two states is equivalent to the two-state translation of the potential-energy landscape in our experiments, and thus would have the effect of translating the walker in the direction of the shorter-lived state. A similar model in which a two-state walker traverses a spatially asymmetric potential-energy landscape yields deterministic motion at higher efficiency than the present model [21]. It does not, however, allow for reversibility. The length of the lever arm and the diffusivity of the motor's body and payload determine the ratio T/τ and thus the motor's efficiency. The two-state ratchet's direction does not depend on T/τ, however, even under heavy loading. This differs from the three-state ratchet [7], in which T/τ also controls the direction of motion. This protocol could be used in the design of mesoscopic motors based on synthetic macromolecules or microelectromechanical systems.

We are grateful for Mark Ofitserov's many technical contributions. This work was supported by the National Science Foundation through Grants No. DBI-0233971 and DMR-0304906. S.L. acknowledges support from the Kessler Family Foundation.

[1] P. Hanggi, ChemPhysChem **3**, 644 (2002).
[2] P. Reimann, Phys. Rep. **361**, 57 (2002).
[3] P. Reimann, Phys. Rev. Lett. **86**, 4992 (2001).
[4] Y.-D. Chen, Phys. Rev. Lett. **79**, 3117 (1997).
[5] R. Kanada and K. Sasaki, J. Phys. Soc. Jpn. **68**, 3759 (1999).
[6] P. H. Jones, M. Goonasekera, and F. Renzoni, Phys. Rev. Lett. **93**, 073904 (2004).
[7] S.-H. Lee, K. Ladavac, M. Polin, and D. G. Grier, Phys. Rev. Lett. **94**, 110601 (2005).
[8] L. P. Faucheux, L. S. Bourdieu, P. D. Kaplan, and A. J. Libchaber, Phys. Rev. Lett. **74**, 1504 (1995).
[9] T. Harada and K. Yoshikawa, Phys. Rev. E **69**, 031113 (2004).
[10] L. I. McCann, M. Dykman, and B. Golding, Nature (London) **402**, 785 (1999).
[11] M. I. Dykman and B. Golding, in *Stochastic Processes in Physics, Chemistry and Biology* edited by J. A. Freund and T. Pöschel (Springer-Verlag, Berlin, 2000), pp. 365–377.
[12] E. R. Dufresne and D. G. Grier, Rev. Sci. Instrum. **69**, 1974 (1998).
[13] J. E. Curtis, B. A. Koss, and D. G. Grier, Opt. Commun. **207**, 169 (2002).
[14] B. A. Koss and D. G. Grier, Appl. Phys. Lett. **82**, 3985 (2003).
[15] H. Risken, *The Fokker-Planck Equation*, 2nd ed. (Springer-Verlag, Berlin, 1989).
[16] E. R. Dufresne, G. C. Spalding, M. T. Dearing, S. A. Sheets, and D. G. Grier, Rev. Sci. Instrum. **72**, 1810 (2001).
[17] Y. Igasaki, F. Li, N. Yoshida, H. Toyoda, T. Inoue, N. Mukohzaka, Y. Kobayashi, and T. Hara, Opt. Rev. **6**, 339 (1999).
[18] S. H. Behrens, J. Plewa, and D. G. Grier, Eur. Phys. J. E **10**, 115 (2003).
[19] J. C. Crocker and D. G. Grier, J. Colloid Interface Sci. **179**, 298 (1996).
[20] K. Kitamura, M. Tokunaga, A. H. Iwane, and T. Yanagida, Nature (London) **397**, 129 (1999).
[21] F. Jülicher, A. Ajdari, and J. Prost, Rev. Mod. Phys. **69**, 1269 (1997).